Supplementary Information Appendix for:

Voltage sensor movements of Cav1.1 during an action potential in skeletal muscle fibers.

Quinton Banks[a], Hugo Bibollet[a], Minerva Contreras[a], Daniel F. Bennett[b], Roger A. Bannister[ab], Martin F. Schneider[a,1] and Erick O. Hernández-Ochoa[a,1]

[a]Department of Biochemistry and Molecular Biology, University of Maryland School of Medicine, Baltimore, Maryland, 21201, United States.

[b]Department of Pathology, University of Maryland School of Medicine, Baltimore, Maryland, 21201, United States.

[1]Corresponding Authors:

Erick Hernández-Ochoa or Martin F. Schneider

108 North Greene Street, Baltimore MD 21201-1503

Phone (410) 706-7812

e-mails: ehernandez-ochoa@som.umaryland.edu or mschneider@som.umaryland.edu

This file includes:

Expanded Material and Methods

Supplementary Figures S1 to S9

Table S1 to S3

Movie S1

SI Appendix

Expanded Materials and Methods

Plasmid Constructs- A plasmid coding for the N-terminal EGFP-tagged of the full-length cDNA coding for the wild-type (WT, EGFP-$Ca_V1.1$) alpha subunit of the $Ca_V1.1$ from rabbit skeletal muscle was used (1, 2). A single cysteine (Cys) was introduced near the extracellular region of each VSD of EGFP-$Ca_V1.1$ (VSDI, construct L159C; VSDII, construct L522C; VSDIII , construct V893C; VSDIV, construct S1231C); to monitor the movement via action potential (AP) fluorometry (see below), a variant of voltage clamp fluorometry (3, 4). Single-point site-directed mutations were generated with QuickChange (Stratagene, Bellingham, WA) and confirmed by sequencing.

In vivo gene transfer via muscle electroporation- Electroporation experiments were carried out on 4-week-old C57BL mice. Experimental protocols were approved by the University of Maryland Institutional Animal Care and Use Committee. The intramuscular injection of various DNA plasmids was conducted, with minor modifications, according to the method of DiFranco et al. (1, 2). Briefly, one footpad of an anesthetized mouse is injected subcutaneously with 20-30 μl of 2 mg/ml hyaluronidase through a 33-gauge needle. 1 to 2 hours later, the mouse is again anesthetized and ~40 μg of plasmid DNA is injected into the footpad. Ten minutes later, two surgical stainless-steel electrodes are placed subcutaneously close to the proximal and distal tendons of the flexor digitorum brevis (FDB) muscle and 20 pulses of 120 V/cm, 20 ms in duration, are applied at 1 Hz via a commercial high current capacity output stage (ECM 830, BTX, Harvard Apparatus, Holliston, MA). Four to six weeks later, single muscle fibers are enzymatically dissociated from the injected FDB muscles and cultured as described below.

Muscle fiber culture- Culture of flexor digitorum brevis (FDB) was carried out as previously described (5, 6). Animals were euthanized by asphyxiation via CO_2 followed by cervical dislocation according to protocols approved by the University of Maryland Institutional Animal Care and Use Committee. Briefly, the FDB muscle was isolated from male adult mice, enzymatically dissociated with collagenase type I (Sigma-Aldrich, St. Louis, MO) in MEM (Life Technologies, Carlsbad, CA) with 10% FBS, and 50 µg/ml gentamicin for 3-4 hours at 37˚ C. Muscle was then gently triturated to separate fibers in MEM with FBS and gentamicin. Fibers were plated in MEM culture media with 10% FBS on glass-bottomed dishes (Matek Cor. Ashland, MA, Cat. No. P35G-1.0-14-C,) coated with laminin (Thermo Fisher, Rockford, IL, Cat. No. 23017-015). Fibers were maintained in culture for 1 to 2 days at 37˚ C, 5% CO_2 prior to the experiments.

Two-electrode voltage clamp (TEVC)- The TEVC was used to measure non-linear capacitive currents and estimate charge movement elicited by an AP waveform or a step-like depolarization. Fibers (<500 µm in length) were choose and visualized on a Zeiss Axiovert 200M inverted microscope. The external recording solution composition was low-Cl^- and Na^+-free (in mM): 150 TEA-CH_3SO_3, 10 HEPES, 0.5 $CaCl_2$, 1 $MgCl_2$, 0.5 $CdCl_2$ and 0.5 $CoCl_2$, 0.001 TTX, 0.5 4-aminopiridine, 0.025 BTS (N-benzyl-p-toluene sulphonamide; Sigma-Aldrich, St Louis, MO, Cat No. 203895), pH adjusted to 7.4 with CsOH. The current injecting electrode (V1) was filled with 2M cesium aspartate and voltage measuring electrode (V2) was filled with 3M cesium chloride as previously described (7). Microelectrode V1 was placed at the middle of the selected fiber, and V2 was positioned halfway between the middle and the end of the selected fiber.

We used an AxoClamp 900A and Axon™ Digidata® 1550B low-noise digitizer (Molecular Devices, San Jose, CA, USA), HS-9A x1 (V1) and HS-9A x0.1 (V2) headstages and borosilicate

glass (Warner Instruments, Cat No. G150TF-3) with resistances of 10–20 MΩ when filled with the electrodes solution. Once the fibers were impaled with both microelectrodes, cells were held at −80 mV. Fibers with signs of clamp error, such as unstable holding current or rapid drifts on holding potential, were rejected from the analysis. Measurements started 5 minutes after TEVC clamp configuration was established. Voltage protocols were generated and current responses were digitized and stored using Clampex and Clampfit (version 11, Molecular Devices, San Jose, CA, USA). Command pulses were delivered at 10 s intervals to the levels and duration indicated in each figure from a holding potential of −80 mV, unless otherwise indicated. Currents were typically low-pass-filtered at 3-10 kHz (3-pole Bessel filter). Currents were sampled at 10 kHz. Linear capacitive and ionic currents were routinely subtracted by a P/5 protocol (8). Gating charge moved during each test depolarization (Q_{ON}) was quantified by calculating the area under the curve of each trace of non-linear current using the post-transient level of each trace as a steady-state value of non-linear ionic current. Total charge moved during repolarization (Q_{OFF}) was calculated similarly (9, 10). Total charge movement was normalized to the linear fiber capacitance, which was determined by measuring linear capacitive current elicited by a ±5 mV test pulse from the holding potential and integrating the area under the capacitive current trace to estimate Q.

Fluorescent probes- Fluo-4 acetoxymethyl (AM) (fluo-4), a membrane-permeable non-ratiometric high affinity Ca^{2+} indicator (Thermo Fisher, Cat. No. F14201), indo-1 acetoxymethyl (AM) (indo-1), a ratiometric high affinity Ca^{2+} indicator (Thermo Fisher, Cat. No. I1203), 4-[2-(6-(dioctylamino)-2-naphthalenyl) ethenyl]-1-(3-sulfopropyl)-, inner salt (di-8-ANEPPS), a membrane-impermeable potentiometric dye (Thermo Fisher, Cat. No. D3167), tetramethylrhodamine-5-maleimide (TMRM) (Thermo Fisher, Cat. No. T6027) and 2-((5(6)-tetramethyl-rhodamine)carboxylamino)ethyl methanethiosulfonate (TAMRA), two membrane-

impermeable sulfhydryl selective compounds (Santa Cruz, Dallas, TX; Cat. No. 329837-19-5). These compounds were dissolved in DMSO.

Fiber staining/loading- Fiber loading with fluo-4 or indo-1 and subsequent imaging and analysis were performed as previously described (11, 12) but with some modifications. Briefly, cultured FDB fibers were loaded with fluo-4AM or indo-1AM (1 μM for 60 min at 22°C) in 1 mL of L-15 media (ionic composition in mM: 137 NaCl, 5.7 KCl, 1.26 CaCl2, 1.8 MgCl2, pH 7.4; Life Technologies, Carlsbad, CA) supplemented with 0.25% w/v bovine serum albumin (BSA; Sigma-Aldrich, St Louis MO, Cat. No. A-7906). Then the fibers were washed thoroughly with appropriate L-15 media to remove residual fluorescent dye. Di-8-ANEPPS dye staining and action potential recordings were performed as previously described but with some modifications (13-16). FDB fibers were stained with 2.5 μM di-8-ANEPPS in the incubator for 3hrs., followed by 2-3 washes in L-15 media before imaging. TAMRA and TMRM staining: control fibers or EGFP-$Ca_V1.1$ transfected fibers were washed 3-5 times in Ringer's solution (ionic composition in mM: 150 NaCl, 4 KCl, 2 CaCl2, 1 MgCl2, 10 HEPES, pH 7.4), to remove cysteines present in the culture media and then primed with 10 μM TAMRA (or TMRM) in Ringer's solution for 4 minutes, to allow the diffusion of Cys-reacting dyes into the TT lumen. Fibers were then repetitively stimulated via remote electrodes in the bath to produce APs at a rate of 50 Hz during 300 ms trains every second for 5 minutes. GLT-myotubes were staining with 10 μM TAMRA in a depolarizing solution for 4 minutes (ionic composition in mM: 155 CsOH, 155 Aspartic acid, 5 Mg Acetate, 10 HEPES, pH 7.4) as described by others (4). Fibers and GLT myotubes were washed 3-5 times in Ringer's to remove unconjugated TAMRA and allowed fiber recovery from (repetitive or sustained) depolarization for 10 min before measurements were obtained. Where noted, BTS (10-50 μM) was added to the recording solution to minimize contractile responses (17). All single fiber

recordings were performed at room temperature, 22°C. Confocal imaging of fluo-4 (100 µs/line), Di-8-ANEPPS (20 µs/line) and TAMRA (200 µs/line) signals were carried out independently using high-speed confocal system LSM 5 Live system (Carl Zeiss, Jena, Germany). Where noted, control fibers or fibers expressing robust EGFP-$Ca_V1.1$ signal were loaded with either fluo-4AM, Di-8-ANEPPS, TAMRA or indo-1AM. Fluo-4 was excited with a 488 nm laser, and the fluorescence emitted >505 mm was detected. Di-8-ANEPPS or TAMRA stained fibers were excited with a 532 nm laser, emitted light was collected with a 550 nm LP filter. Indo-1 was excited with a 405 nm laser, and the fluorescence emitted between 420-460 nm was detected. Fluo-4, Di-8-ANEPPS or TAMRA stained fibers were viewed on a Zeiss Axiovert 200M inverted microscope and confocal imaging was performed in line scan *xt* mode as previously described (13-15), with images acquired for 0.4 to 1 s, using a 63x 1.2 N.A. water immersion objective. Indo-1 and TAMRA presented in supplemental figure S6, S9 and Movie S1 were viewed on a Fluoview 3000 inverted microscope (Olympus, Tokyo, Japan) and confocal video and line scan recording were performed in *xy* (30 fps, 512-512 pixel frame) and *xt* (126 µs/line) mode respectively, using a 40x 1.2 N.A. oil immersion objective.

Calculation of SR Ca^{2+} release flux from fluo-4 fluorescence recordings- Fluo-4 fluorescence recordings (F) and baseline fluorescence (F0) were converted to ratio signals [R = (F − F0)/F0] as previously described (16, 18). A Ca^{2+} removal model including binding and transport was used to estimate the time course of the Ca^{2+} release flux during action potential induced activation as described (19, 20). Binding to Ca^{2+}-specific sites of troponin C (T-sites) and parvalbumin-like Ca^{2+}-Mg^{2+} sites (P-sites), as well as fast Ca^{2+} binding to ATP was calculated using binding site concentrations, rate constants and approximations adopted from previous reports (16, 18, 19). The fixed rate constant values used for the calculations were for T-sites: kon, T, Ca = 115 µM/sec, koff,

T, Ca = 150/sec; and for P-sites: kon,P,Ca = 54.0 μM/sec, koff, P, Ca = 0.65/sec, kon, P, Mg = 0.043 μM/sec, koff, P, Mg = 3.9/sec, kuptake = 1000/sec. [T]tot and [P]tot, the total concentrations of T-sites and P-sites, were 0.240 mmol/L and 1.5 mmol/L, respectively. After an initial calculation with these parameters, kon, P, Mg, and kuptake were adjusted by iteration to minimize the least squares deviation between calculated and measured fluorescence ratio. The Ca^{2+} occupancies of all model compartments [T-sites, P-sites, ATP (F-sites), and uptake] were summed, and the release flux was calculated as the time derivative of the sum (21). Calculations were performed using Euler's method (22). Analysis was performed using Excel Solver (Microsoft).

Approximation of SR Ca^{2+} release flux from indo-1 fluorescence recordings- Indo-1 fluorescence recordings (F) and baseline fluorescence (F0) were converted to ratio signals [R = − (F − F0)/F0] as previously described (16, 18). The rate of Ca^{2+} release flux was roughly approximated by the first derivative of the optically recorded and uncorrected indo1 transient.

Field stimulation- Electrical field stimuli were applied via two parallel platinum wires closely spaced (5 mm). Application of each stimulation protocol was synchronized relative to the start of fluorescence acquisition. Each stimulating pulse (1 ms, 10-20 V/cm) was delivered alternating the polarity using a custom pulse generator. Only fibers responding with action potential-induced twitch responses for both polarity stimulation before and after staining were studied (13, 23). Typically, the field stimuli were applied 100 ms after the start of the recording confocal scan sequence, thus providing control images before stimulation at the start of each sequence. These control images segments were used to determine the resting steady-state fluorescence level (F0). Average intensity of fluorescence within the selected optical field was recorded and background corrected by subtracting an average value recorded outside the cell. The average F0 value in each

trace before electrical stimulation was used to scale fluorescent signals (fluo-4, Di-8-ANEPPS, TAMRA and indo-1) in the same field as ΔF/F0 or −ΔF/F0.

In a different set of experiments control (non-transfected) and EGFP-$Ca_V1.1$ fibers were stained with TAMRA (5 μM; in Ringer's solution) and imaged on a Fluoview 500 confocal system (Olympus; ×60, 1.3 NA water-immersion objective; pixel dimensions 0.2 × 0.2 μm in *x* and *y*). Confocal images were obtained with 512 × 512 pixel *xy* images (average of eight images). The excitation for EGFP and TAMRA were provided by using 488 and 532 nm lasers, respectively. The emitted light for EGFP was collected using a 505-525 nm band filter. TAMRA emission was collected using 550 nm long-pass filter.

$Ca_V1.1$ immunostaining- Immunostaining was performed as previously reported (5, 12, 15). Cultures FDB fibers were rinsed in PBS, and then incubated with 4% PFA in PBS for 20 minutes. Then rinsed with PBS 3 times. Afterwards, incubated in 0.5 % Triton X-100 in PBS for 20 minutes and rinsed with PBS 3 times. Goat serum 8% in PBS was used as blocking agent (Thermo-Scientific, Rockford, IL, Cat No. 31872) for 1 hour on a shaker. After blockage, fibers were incubated with primary antibody for $Ca_V1.1$ (Invitrogen, Carlsbad, CA, Cat No. MA3-920) at a 1:200 concentration in 2% goat serum in PBS for 48 hours. Secondary antibody (Invitrogen, Carlsbad, CA, Goat-anti mouse AlexaFluor 633, Cat No. A-21052) was defrosted, spun down at 4º C at 10,000 rpm, and diluted (1:250) into 2% goat serum in PBS. Cells were incubated with secondary antibody in cold room for 3 hours. After incubation, cells were washed 5 times with PBS. Inmunostained cells were viewed on a Fluoview 500 inverted microscope (Olympus, Tokyo, Japan). Images of 512-512 pixel were acquired using a 20x 0.5 N.A. objective. The excitation for EGFP and Alexa-Fluor 633-conjugated antibody were provided by using 488 and 633 nm lasers, respectively. The emitted light for EGFP was collected using a 505-525 nm band filter. Alexa-

Fluor 633 emission was collected using 660 nm long-pass filter. Images were collected from randomly selected fibers using the same image acquisition settings and enhancing parameters. Images were background corrected and a region of interest of fixed dimensions was used to estimate average fluorescence profile within the region of interest.

GLT culture- Myoblasts of the dysgenic (mdg/mdg) cell line GLT (A gift from Dr. Bernard Flucher; passage 24 to 30) were cultured at 37°C in 5% CO_2 in growing media (10% FBS, 10% horse serum (HS), DMEM, PenStrep 100U/ml) on 35-mm plastic culture dishes (Corning, Tewksburry MA, USA, Cat. No. 353801). Growing media was change at ~90% cells confluency (day 2-3) to fusion media (2% HS, DMEM, PenStrep 100U/ml) and was changed daily until experimentation (day 7-9). Transfection occurred day 4 after plating using FuGENE-HD transfection reagent (Promega, Madison WI, USA, Cat. No. E2311). Cells were placed at 30°C in 5% CO_2 incubator in fusion media 1 day before experimentation. Since GLT myotubes endogenously express all the auxiliary subunit of $Ca_V1.1$ (i.e., α2δ-1, β1a, and γ1) as well as STAC3 and RyR type-1 (24-26), only $Ca_V1.1$ EGFP N-termini tagged constructs were transfected. Transfection ratio were 6 ul FuGENE-HD for 2µg cDNA by 35mm dish. Transfected myotubes were identified by EGFP fluorescence using epifluorescence microscopy, excited at 488 ±10 nm with a xenon lamp, and the fluorescence emitted >505 nm.

GLT patch clamp- Currents were recorded by patch-clamp technique in whole-cell configuration using an Axopatch 200B amplifier (Molecular Devices, San Jose, CA, USA). Patch pipettes had resistances between 2.0 to 3.5 MΩ (borosilicate glass; Harvard Apparatus) and were filled with (mM) 145 Cs-aspartate, 2 MgCl2,10 HEPES and 0.1 Cs-EGTA (pH 7.4 with CsOH). For calcium currents recording, GLT myotubes were bathed in external solution containing (mM) 10 CaCl2, 145 tetraethylammonium-chloride, and 10 HEPES (pH 7.4 with tetraethylammonium hydroxide).

Charge movement were recorded in a similar solution with addition (mM) 0.1 LaCl3 and 0.5 CdCl2. Data were acquired with pCLAMP software (version 9.2; Molecular Devices, San Jose, CA, USA). Electronic compensation was used to reduce the effective series resistance (~80%). Linear components of leak and capacitive currents were corrected with −P/4 online subtraction protocols. Filtering was 5 kHz and digitization was at 10 kHz. Cell capacitance (Cm) was determined by integration of a transient from holding potential (−80 mV) to −70 mV and was used to normalize current amplitudes (pA/pF).

Data analysis and statistics methods- To avoid one source of systematic bias, experimental and control measurements were alternated whenever possible and concurrent controls were always performed. Because EGFP-$Ca_V1.1$ expression tended to be non-uniform over the fiber, the linescan TAMRA recordings were taken at different positions in each fiber, which were consequently activated at different times after the initiation of a propagated AP at one end or the other end of a fiber, as occurs with remote electrode bipolar stimulation (13, 23). VSD fluorescence time course data were acquired in LSM 5 Live (Zeiss, Jena, Germany). Data spreadsheets were generated from the raw fluorescent images. Data were initially processed in Excel (Microsoft, Redmond, WA, USA). Visual Basic (Microsoft, Redmond, WA, USA) macros were used to systematically determine the $\Delta F/F0$ or $-\Delta F/F0$ values. Data were then analyzed and plotted using OriginPro 2020b (OriginLab Corporation, Northampton, MA, USA). In order to achieve synchronized averaging of VSD signals, VSD fluorescence time course records were shifted along the time axis. This shifting was carried out after taking recordings utilizing bipolar field stimulation. By using alternate polarity stimulation to obtain recordings with APs initiated at either end, we obtain VSD recordings with slightly different initiation times relative to the stimulus time. To obtain an averaged estimation of the time course, we shifted the recordings from each end to the average of

their 50 % rise times (i.e., split the difference in rise time between the recordings). After this was done for each fiber, we averaged the fiber mean time courses together to obtain the overall average trace of each VSD initiation. Graphs were then normalized to the peak value.

AP (taken with Di-8-ANEPPS) and Ca^{2+} transients (taken with fluo-4 or indo-1) were handled in a similar fashion to the VSD recordings (LSM → Excel → Origin). Because the fluorescence from Di-8-ANEPPS, fluo-4 and indo-1 were uniform over the fiber, records were taken in the middle of the fiber and no temporal shifting was needed. Before plotting with the VSD signals, the peaks of the traces were normalized to 1. LSM 5 Live and TTL marker on the linescan image signifying the field stimulation pulse turning off (1 ms pulse). The precision of the marker location was tested and corroborated using an LED activated with the +5 V TTL signal, with a variability <100 µs between the trials. Using the marker, we set time 0 on our Origin generated graphs to 1 ms before the marker appears in our LSM5Live recordings.

TAMRA and EGFP-$Ca_V1.1$ *xy* images were analyzed with ImageJ (National Institutes of Health, Bethesda, MD; http://rsb.info.nih.gov/ij/).

Muscle fiber and GLT myotube membrane current analysis- Data analysis was performed using Clampfit 8.0 (Molecular Devices, San Jose, CA, USA). Further data evaluation, non-linear fitting and statistical analysis were conducted using OriginPro 2020b software. The I–V plots from GLT myotubes were fitted to a Boltzmann-Ohmic function, described by the following equation (27):

$$\boldsymbol{I(V) = G_{max}(V - V_{rev})/[1 + exp\,(-(V - V_{half}/k]},$$

where G_{max} is the maximum conductance, V is the membrane potential, V_{rev} is the reversal potential, V_{half} is the half-activation potential, and k is a measure of the steepness. Average Ca^{2+}

conductance Boltzmann's parameter values for V_{half} and k for the different channel constructs used here are shown in Table 1.

Similarly, the Q-V relationship of each individual fiber or GLT myotube was fitted to a single Boltzmann function, as described by the equation:

$$\boldsymbol{Q(V) = Q_{max}/(1 + exp\,((V_{half} - V)/k))},$$

where Q_{max} gives the maximum charge movement, V_{half} defines the potential where Q = 0.5 of Q_{max} and $1/k$ is a measure of the steepness of the Q–V relationship. Average Q_{ON} Boltzmann's parameter values for V_{half} and k for the channel constructs used here are shown in Table 2.

Q-t relationship of each individual GLT myotube was obtained by integration of the Q_{ON} from t=0 to t=10 ms (end of the Q_{ON} phase in all recordings) elicited by a single 20 ms depolarizations from −50 to +50 mV (saturation of the Q-V). Q-t were normalized by maximum value, obtained at t=10ms. Residual leak currents were subtracted from each individual trace by a square-like function before analysis to allow kinetic comparisons. Average Q_{ON} parameter values for t_{half} (time were Q = 0.5 Q_{ONmax}) and $\Delta t_{20\text{-}80}$ (time to reach Q = 0.8 Q_{ONmax} from Q = 0.2 Q_{ONmax}) for each channel constructs were determined graphically and averaged. Results are shown in Table 3.

Statistical analysis- Normal distribution of data was assessed using the Kolmogorov–Smirnov test. Summary data were reported as mean ± SEM except when mentioned (see figure legend) when samples followed normal distributions, and as medians when sample distributions were less well defined. Statistical significance was assessed using either parametric two sample t-test, non-parametric Mann-Whitney rank-sum test, or one-way ANOVA followed by Tukey-Kramer *post hoc* for unpaired data sets and paired t-Test for paired data sets. Differences were considered significant when p-value <0.05.

References

1. M. DiFranco, M. Quinonez, J. Capote, J. Vergara, DNA transfection of mammalian skeletal muscles using in vivo electroporation. *J Vis Exp* 10.3791/1520 (2009).
2. M. DiFranco, P. Tran, M. Quinonez, J. L. Vergara, Functional expression of transgenic 1sDHPR channels in adult mammalian skeletal muscle fibres. *J Physiol* **589**, 1421-1442 (2011).
3. L. M. Mannuzzu, M. M. Moronne, E. Y. Isacoff, Direct physical measure of conformational rearrangement underlying potassium channel gating. *Science* **271**, 213-216 (1996).
4. A. Pantazis, N. Savalli, D. Sigg, A. Neely, R. Olcese, Functional heterogeneity of the four voltage sensors of a human L-type calcium channel. *Proc Natl Acad Sci U S A* **111**, 18381-18386 (2014).
5. E. O. Hernández-Ochoa *et al.*, Elevated extracellular glucose and uncontrolled type 1 diabetes enhance NFAT5 signaling and disrupt the transverse tubular network in mouse skeletal muscle. *Exp Biol Med (Maywood)* **237**, 1068-1083 (2012).
6. Y. Liu, S. L. Carroll, M. G. Klein, M. F. Schneider, Calcium transients and calcium homeostasis in adult mouse fast-twitch skeletal muscle fibers in culture. *Am J Physiol* **272**, C1919-1927 (1997).
7. Y. Fu, A. Struyk, V. Markin, S. Cannon, Gating behaviour of sodium currents in adult mouse muscle recorded with an improved two-electrode voltage clamp. *J Physiol* **589**, 525-546 (2011).
8. C. M. Armstrong, F. Bezanilla, Charge movement associated with the opening and closing of the activation gates of the Na channels. *J Gen Physiol* **63**, 533-552 (1974).
9. B. L. Prosser, E. O. Hernandez-Ochoa, D. B. Zimmer, M. F. Schneider, The Qgamma component of intra-membrane charge movement is present in mammalian muscle fibres, but suppressed in the absence of S100A1. *J Physiol* **587**, 4523-4541 (2009).
10. M. F. Schneider, W. K. Chandler, Voltage dependent charge movement of skeletal muscle: a possible step in excitation-contraction coupling. *Nature* **242**, 244-246 (1973).
11. P. Robison *et al.*, Impaired calcium signaling in muscle fibers from intercostal and foot skeletal muscle in a cigarette smoke-induced mouse model of COPD. *Muscle Nerve* **56**, 282-291 (2017).
12. B. L. Prosser *et al.*, S100A1 binds to the calmodulin-binding site of ryanodine receptor and modulates skeletal muscle excitation-contraction coupling. *J Biol Chem* **283**, 5046-5057 (2008).
13. Q. Banks *et al.*, Optical Recording of Action Potential Initiation and Propagation in Mouse Skeletal Muscle Fibers. *Biophys J* **115**, 2127-2140 (2018).
14. E. O. Hernandez-Ochoa, S. J. Pratt, K. P. Garcia-Pelagio, M. F. Schneider, R. M. Lovering, Disruption of action potential and calcium signaling properties in malformed myofibers from dystrophin-deficient mice. *Physiol Rep* **3** (2015).
15. E. O. Hernandez-Ochoa, T. N. Schachter, M. F. Schneider, Elevated nuclear Foxo1 suppresses excitability of skeletal muscle fibers. *Am J Physiol Cell Physiol* **305**, C643-653 (2013).
16. B. L. Prosser *et al.*, S100A1 promotes action potential-initiated calcium release flux and force production in skeletal muscle. *Am J Physiol Cell Physiol* **299**, C891-902 (2010).
17. J. Bruton, G. J. Pinniger, J. Lannergren, H. Westerblad, The effects of the myosin-II inhibitor N-benzyl-p-toluene sulphonamide on fatigue in mouse single intact toe muscle fibres. *Acta Physiol (Oxf)* **186**, 59-66 (2006).
18. N. Yamaguchi *et al.*, Modulation of sarcoplasmic reticulum Ca2+ release in skeletal muscle expressing ryanodine receptor impaired in regulation by calmodulin and S100A1. *Am J Physiol Cell Physiol* **300**, C998-C1012 (2011).
19. S. M. Baylor, S. Hollingworth, Sarcoplasmic reticulum calcium release compared in slow-twitch and fast-twitch fibres of mouse muscle. *J Physiol* **551**, 125-138 (2003).
20. W. Melzer, E. Rios, M. F. Schneider, A general procedure for determining the rate of calcium release from the sarcoplasmic reticulum in skeletal muscle fibers. *Biophys J* **51**, 849-863 (1987).
21. J. Timmer, T. Muller, W. Melzer, Numerical methods to determine calcium release flux from calcium transients in muscle cells. *Biophysical journal* **74**, 1694-1707 (1998).

22. J. B. Scarborough, *Numerical Mathematical Analysis* (Johns Hopkins Press Baltimore, ed. 6th, 1966).
23. E. O. Hernandez-Ochoa, C. Vanegas, S. R. Iyer, R. M. Lovering, M. F. Schneider, Alternating bipolar field stimulation identifies muscle fibers with defective excitability but maintained local Ca(2+) signals and contraction. *Skeletal muscle* **6**, 6 (2016).
24. E. Rios, G. Brum, Involvement of dihydropyridine receptors in excitation-contraction coupling in skeletal muscle. *Nature* **325**, 717-720 (1987).
25. T. Tanabe, K. G. Beam, J. A. Powell, S. Numa, Restoration of excitation-contraction coupling and slow calcium current in dysgenic muscle by dihydropyridine receptor complementary DNA. *Nature* **336**, 134-139 (1988).
26. Y. El Ghaleb, M. Campiglio, B. E. Flucher, Correcting the R165K substitution in the first voltage-sensor of Cav1.1 right-shifts the voltage-dependence of skeletal muscle calcium channel activation. *Channels (Austin)* **13**, 62-71 (2019).
27. J. Nakai *et al.*, Enhanced dihydropyridine receptor channel activity in the presence of ryanodine receptor. *Nature* **380**, 72-75 (1996).

Supplementary figures

Figure S1. Step voltage clamp P/5 leak subtraction protocol. A) P/5 voltage steps elicited from a −120 mV subholding potential, B) P/5 current leak templates, C) test pulse (P) to +20 mV from a −80 mV holding potential, D) total current in response to P, E) P (orange trace) and P/5 pulse (cyan trace), F) total current (I total, orange trace) elicited by P, current leak template (I leak, cyan trace; sum of P/5 leak responses) and asymmetric current (red trace; I total−I leak). Note that in panel B and D, the current zero offset was subtracted.

Figure S2. Action potential (AP) voltage clamp AP/5 leak subtraction protocol. A) AP/5 voltage waveforms elicited from a −120 mV subholding potential, B) AP/5 current leak templates, C) AP waveform from a −80 mV holding potential, D) total current in response to AP waveform, E) AP (orange trace) and AP/5 waveform (cyan trace), F) total current (I total, orange trace) elicited by AP waveform, current leak template (I leak, cyan trace; sum of AP/5 leak responses) and asymmetric current (red trace; I total− I leak). Note that in panel B and D, the current zero offset was subtracted.

Figure S3. Average and individual AP-induced TAMRA fluorometric signals recorded from each Cys-engineered Cav1.1 constructs. TAMRA fluorometric (mean ± SEM) signals were taken from separate populations of FDB fibers. A) VSDI (construct L159C), B) VSDII (construct L522C), C) VSDIII (construct V893C), D) VSDIV (construct S1231C). APs were delivered via field stimulation at t = 0. The fibers were treated with BTS to reduce contraction but note that some recordings are still subjected to the movement artifact, explaining the signal

drop below baseline after the peak, and average signal decay phase variability. TAMRA signal peak −ΔF/F0 for all VSDs ranged from 0.008-0.03. Please note that VSDII records included one fiber with a large movement signal. However, removing this fiber from the average hardly affected the rising phase or the peak of the average VSDII signal, but did alter the decaying phase.

Figure S4. Cys mutations and $Ca_V1.1$ properties: Ca^{2+} currents. Exemplar records of L-type Ca^{2+} currents elicited by 200 ms depolarizations (from −40 to +60 mV; colored trace indicates maximum inward current), preceded by 1 sec prepulse to −30 mV from a holding potential set at −80 mV and recorded from GLT-myotubes expressing EGFP-$Ca_V1.1$ WT (far left) or Cys-engineered VSDs: VSDI (construct L159C, left), VSDII (construct L522C, middle), VSDIII (construct V893C, right), VSDIV (construct S1231C, far right). B) I *vs.* V relationship of each of the individual VSD Cys-modified channels fitted to a Boltzmann-Ohmic function (see *SI Appendix, Expanded Materials and Methods*). Values are expressed as mean ±SEM, (n=5-11). C) G *vs.* V relationships extrapolated from I *vs.* V fits parameters presented in B. Boltzmann parameters are shown in *SI Appendix* Table S1.

Figure S5. Cys mutations and $Ca_V1.1$ properties: gating currents and charge movement. A) Exemplar records of non-linear capacitive currents elicited by 20 ms depolarizations (from −40 to +50 mV) preceded by 1 sec prepulse to −30 mV from a holding potential set at −80 mV and recorded from GLT-myotubes expressing EGFP-$Ca_V1.1$ WT (far left) or Cys-engineered VSDs: VSDI (construct L159C, left), VSDII (construct L522C, middle), VSDIII (construct V893C, right) and VSDIV (construct S1231C, far right). Overlapped traces indicate step pulse

depolarization from −50 to +50 mV. B) Q *vs.* V relationship of each of the individual VSD Cys-modified channels fitted to a single Boltzmann function. Values are expressed as mean ±SEM. Q_{ON} established by integrating non-linear current traces during 20 ms pulse (see *SI Appendix, Expanded Materials and Methods*). Values are expressed as mean ±SEM, (n=4-9). Boltzmann parameters are shown in *SI Appendix* Table S2.

Figure S6. Cys mutations and $Ca_V1.1$ properties in presence Cys-reacting fluorophore labeling (TAMRA): gating currents and charge movement. A) Representative non-linear capacitive currents elicited by 20 ms depolarizations from −50 to +50 mV preceded by 1 sec prepulse to −30 mV from a holding potential set at −80 mV and recorded from GLT-myotubes expressing Cys-engineered without (grey) or with TAMRA staining: VSDI (construct L159C, purple), VSDII (construct L522C, cyan), VSDIII (construct V893C, red) and VSDIV (construct S1231C, blue). Note that the traces in the absence of TAMRA staining are the same as the ones presented in figure S5. Residual leak currents were subtracted from each individual trace by a square like function to allow kinetic comparisons between stained and non-stained myotubes (see *SI Appendix, Expanded Materials and Methods*). B) Q *vs.* V relationship of each of the individual VSD Cys-modified channels without (black) or with TAMRA staining, color coded as in A, fitted to a single Boltzmann function. Q_{ON} estimated by integrating non-linear current traces during 20 ms pulse from −40 to +60 mV from a subholding potential to –50mV (see *SI Appendix, Expanded Materials and Methods*). Values are expressed as mean ±SEM, (n=3-5). Boltzmann parameters are shown in *SI Appendix* Table S2. C) Q *vs.* t relationship (Q-t) of WT (dashed line) and individual VSD Cys-modified channels without (black) or with TAMRA staining, colored as in A, elicited by a 20 ms depolarizations from −50 to +50 mV. Q_{ON} estimated

by integrating non-linear current traces from 0 to 10ms. Each recording was normalized by the value of Q_{ON} at 10ms (see *SI Appendix, Expanded Materials and Methods*). Values are expressed as mean ±SEM, (n=3-5). Rise time to Q50% ($t_{1/2}$) and time between Q20-80% (Δt_{20-80}) parameters are shown in *SI Appendix* Table S3. TAMRA did not affect the kinetics or the voltage dependence of the gaiting currents of Cys-engineered $Ca_V1.1$.

Figure S7. TAMRA staining and repetitive stimulation protocol do not affect action potential induced muscle contraction in FDB muscle fibers expressing a Cys-engineered EGFP-Cav1.1, nor the fiber morphology. Representative transmitted and confocal picture of FDB fibers electroporated with EGFP-$Ca_V1.1$ L522C (VSDII) plasmid, before TAMRA staining protocol (A), directly after stimulation but before TAMRA washout (B), and 10 minutes after washout and stimulation protocol. Details of staining and repetitive stimulation protocol can be found in *SI Appendix*. Corresponding movie S1 showing twitch response to field stimulation for panel A-C can be found in *SI Appendix.* D) Representative EGFP, TAMRA and transmitted light signals from fiber shown in panel A to C. TAMRA staining does not affect excitability and morphology of isolated muscle fibers expressing Cys-engineered $Ca_V1.1$ channel.

Figure S8. TAMRA staining and repetitive stimulation protocol do not affect action potential induced-calcium transient in FDB muscle fibers expressing a Cys-engineered EGFP-Cav1.1. A) Transmitted (far left) and confocal images of EGFP signal (left), before (middle) and after TAMRA staining (right), and indo-1 at rest (far right) of a muscle fiber electroporated with EGFP-$Ca_V1.1$ L522C (VSDII) plasmid, scale bars 20 µm. Line scan fluorescent profile of indo-1 signals

of FDB fiber shown in A before (Top) and after (Bottom) TAMRA staining and stimulation protocol (B). Superimposed traces show the average time fluorescent profile. Red arrow indicates single field stimulation. Details of staining and repetitive stimulation protocol can be found in *SI Appendix*. C) Top: Average (±SEM) −ΔF/F0 signal before (black) and after (red) TAMRA staining and stimulation protocol, elicited by a single field stimulation pulse. Bottom: Box plot summarizing data from top panel C. No significant difference in peak amplitude (p=0.13) or time to peak (p=0.75) for −ΔF/F0 were observed (n=7), paired sample t-Test. D) Top: Average (±SEM) of first derivative of −ΔF/F0 signal, to roughly approximated the release flux rate, before (black) and after (red) TAMRA staining, and stimulation protocol elicited by a single field stimulation pulse. Bottom: Box plot summarizing data from top panel D. No significant difference in peak of the derivative (p=0.28) (n=7), paired sample t-Test. In C and D, box upper and lower limits represent the 75th and 25th percentiles, respectively; the whiskers indicate ± S.D. Details of staining and stimulation protocol, and calcium release approximation from indo-1 measurements can be found in *SI Appendix*.

Figure S9. Cys-reacting fluorophore labeling (TAMRA) caused negligible effects on non-linear capacitive currents and charge movement in untransfected FDB muscle fibers. Representative non-linear capacitive currents from a control untransfected fiber before (A) and after (B) 4 min exposure to 5 μM TAMRA in the recording chamber. Non-linear capacitive currents were elicited by 25 ms depolarizations (from −60 to +60 mV) from a holding potential set at −80 mV. C) Q *vs.* V relationship of 4 control fibers before and after treatment with TAMRA. The Q-V relationships were fitted to a single Boltzmann function with the following parameters: Q_{max}= 33.1 nC/μF, V_{half}= −13.9 mV and k= 22.7 mV for control fibers and Q_{max}= 31.7 nC/μF, V_{half}=

−15.5 mV and *k*= 23.35 mV for TAMRA treated fibers. TAMRA did not affect the amplitude, kinetics, and voltage dependence of the charge movement in untransfected muscle fibers.

Movie S1. TAMRA staining and repetitive stimulation protocol do not affect action potential induced muscle contraction in FDB muscle fibers expressing a Cys-engineered Cav1.1. Representative transmitted and confocal video of FDB fiber electroporated with EGFP-$Ca_V1.1$ L522C (VSDII) plasmid, before TAMRA staining protocol (left), directly after repetitive stimulation but before TAMRA washout (middle), and 10 min after washout and repetitive stimulation protocol (right). Stimulation was applied at different times after beginning of image series. Note that the field stimulation elicited-twitch was qualitatively similar before and 10 minutes after stimulation and TAMRA washout, indicating that these procedures are not affecting the fiber's excitability and contractility. Details of staining and repetitive stimulation protocol can be found in *SI Appendix*.

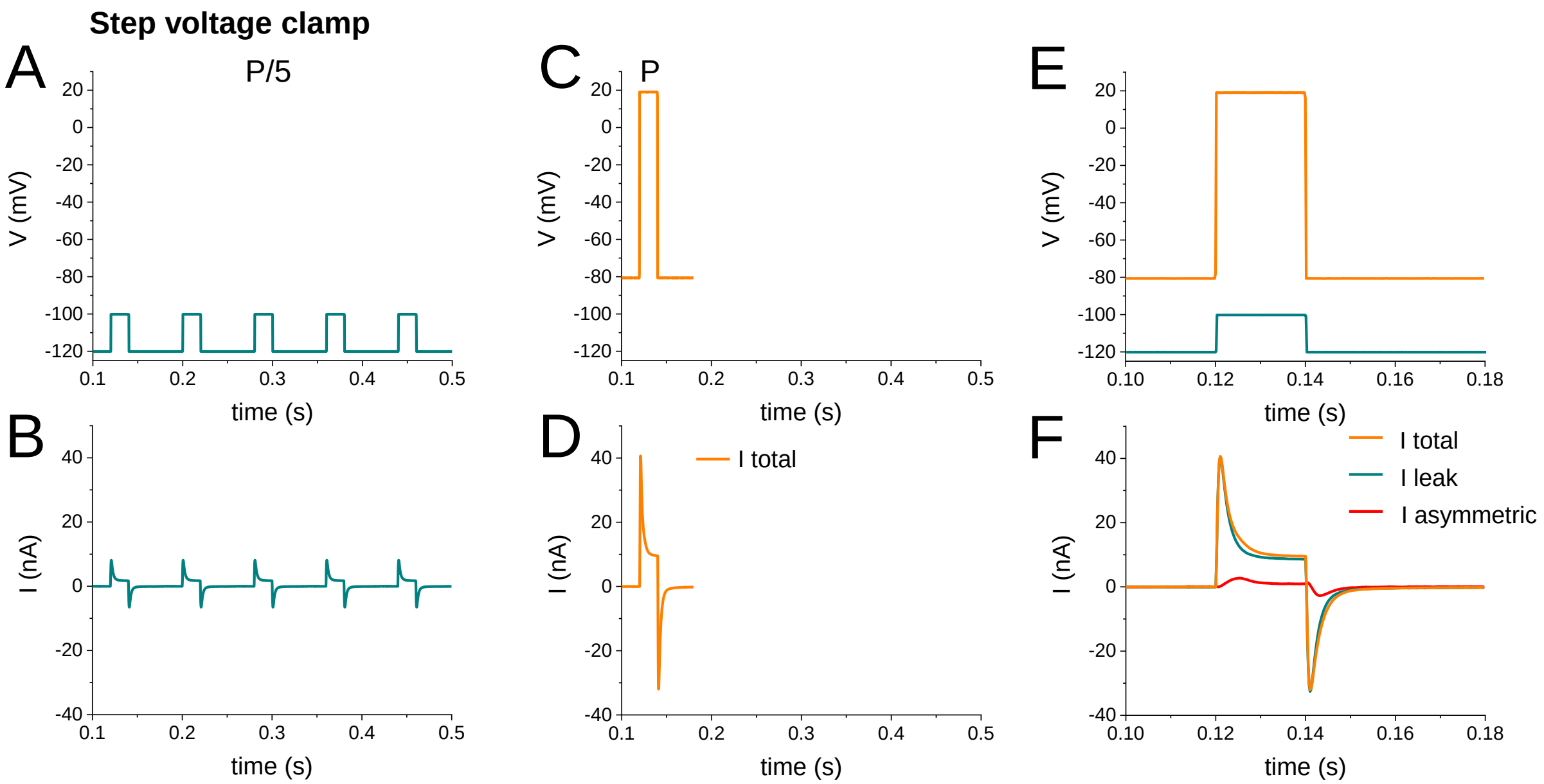
Step voltage clamp
A
P/5
V (mV)
time (s)
B
I (nA)
time (s)
C
P
V (mV)
time (s)
D
I total
I (nA)
time (s)
E
V (mV)
time (s)
F
I total
I leak
I asymmetric
I (nA)
time (s)

Figure S1

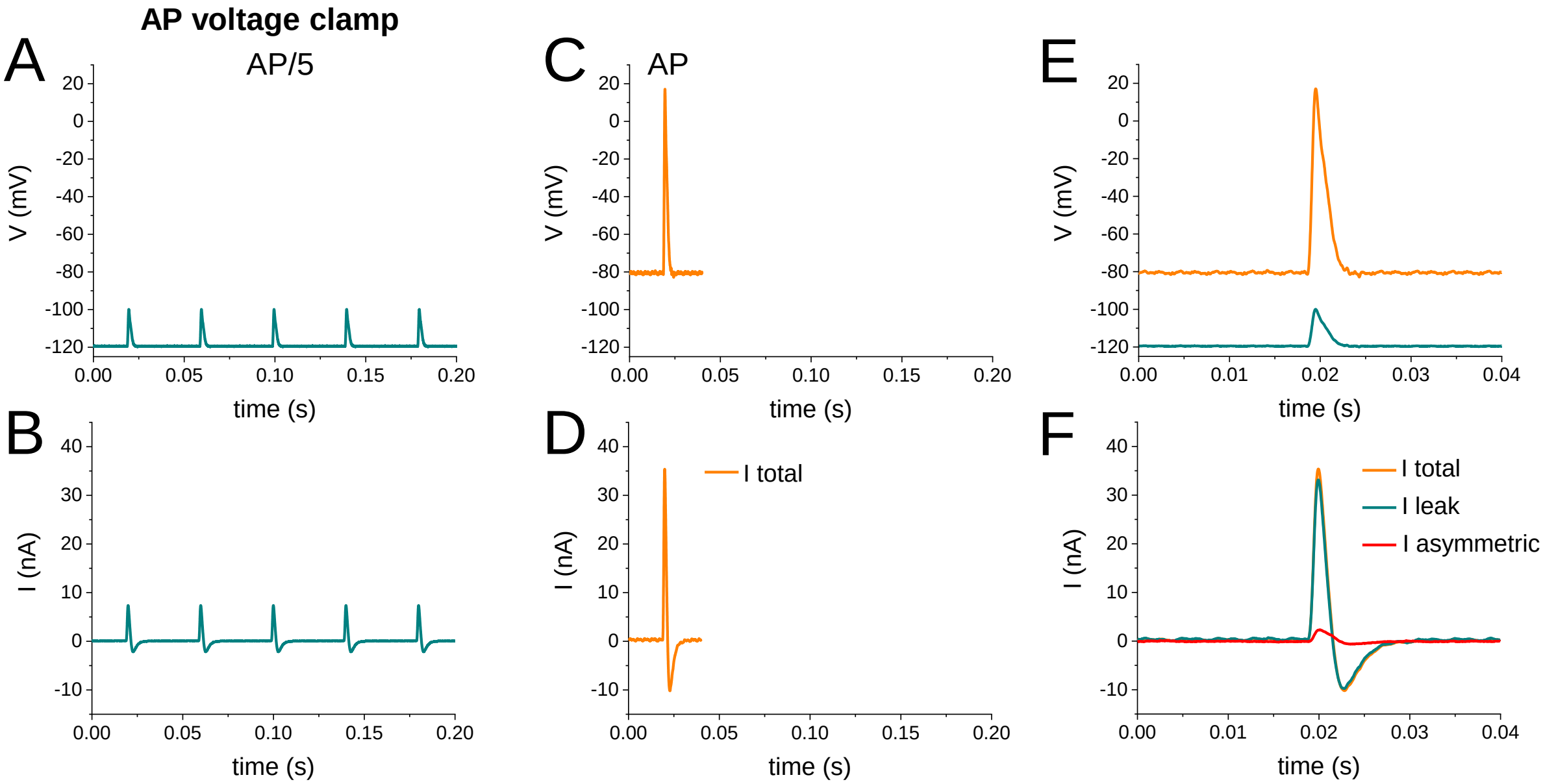
AP voltage clamp
A
AP/5
V (mV)
time (s)
B
I (nA)
time (s)
C
AP
V (mV)
time (s)
D
I total
I (nA)
time (s)
E
V (mV)
time (s)
F
I total
I leak
I asymmetric
I (nA)
time (s)

Figure S2

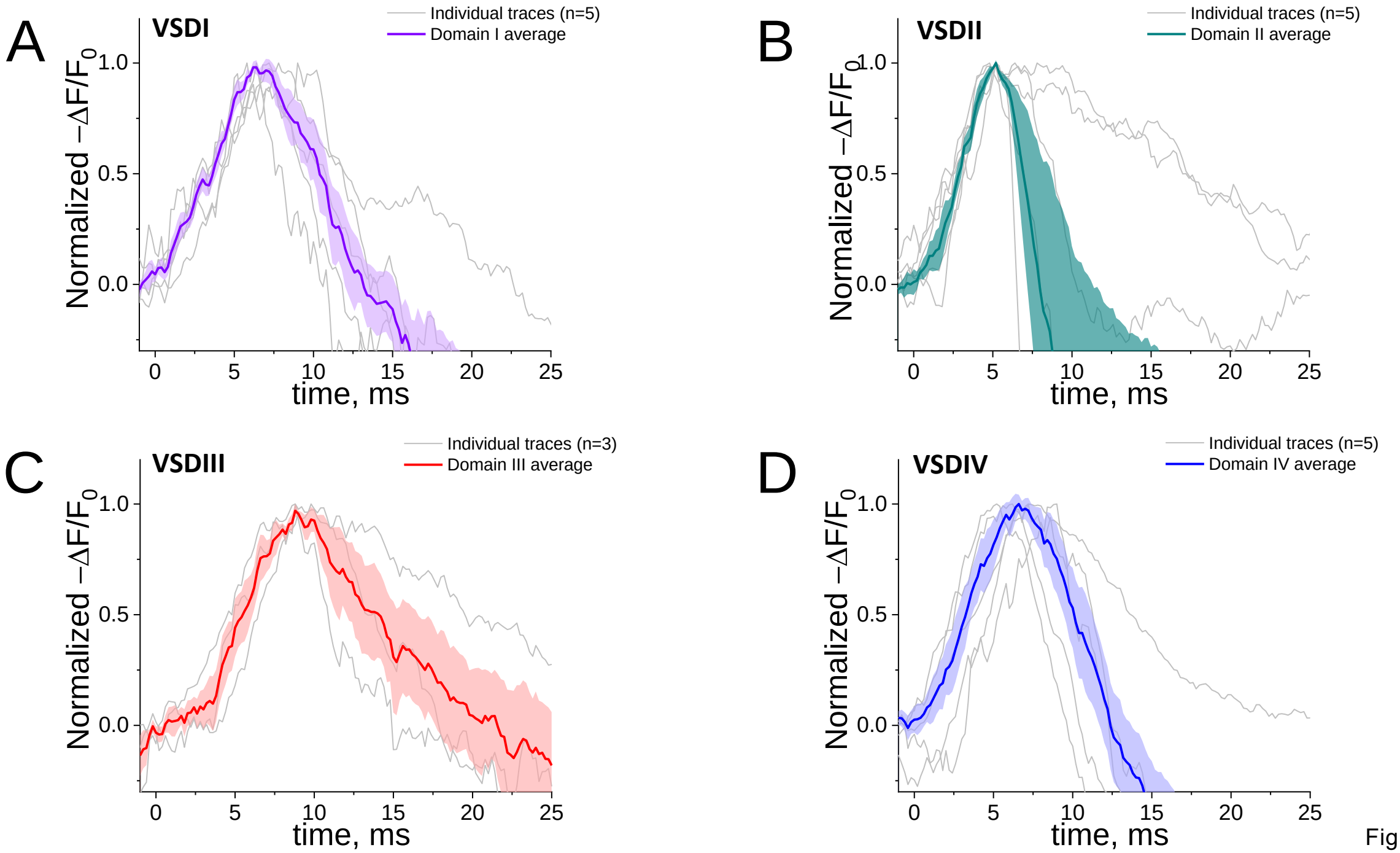
A
VSDI
Individual traces (n=5)
Domain I average
Normalized −ΔF/F0
1.0
0.5
0.0
0
5
10
15
20
25
time, ms
B
VSDII
Individual traces (n=5)
Domain II average
Normalized −ΔF/F0
1.0
0.5
0.0
0
5
10
15
20
25
time, ms
C
VSDIII
Individual traces (n=3)
Domain III average
Normalized −ΔF/F0
1.0
0.5
0.0
0
5
10
15
20
25
time, ms
D
VSDIV
Individual traces (n=5)
Domain IV average
Normalized −ΔF/F0
1.0
0.5
0.0
0
5
10
15
20
25
time, ms

Figure S3

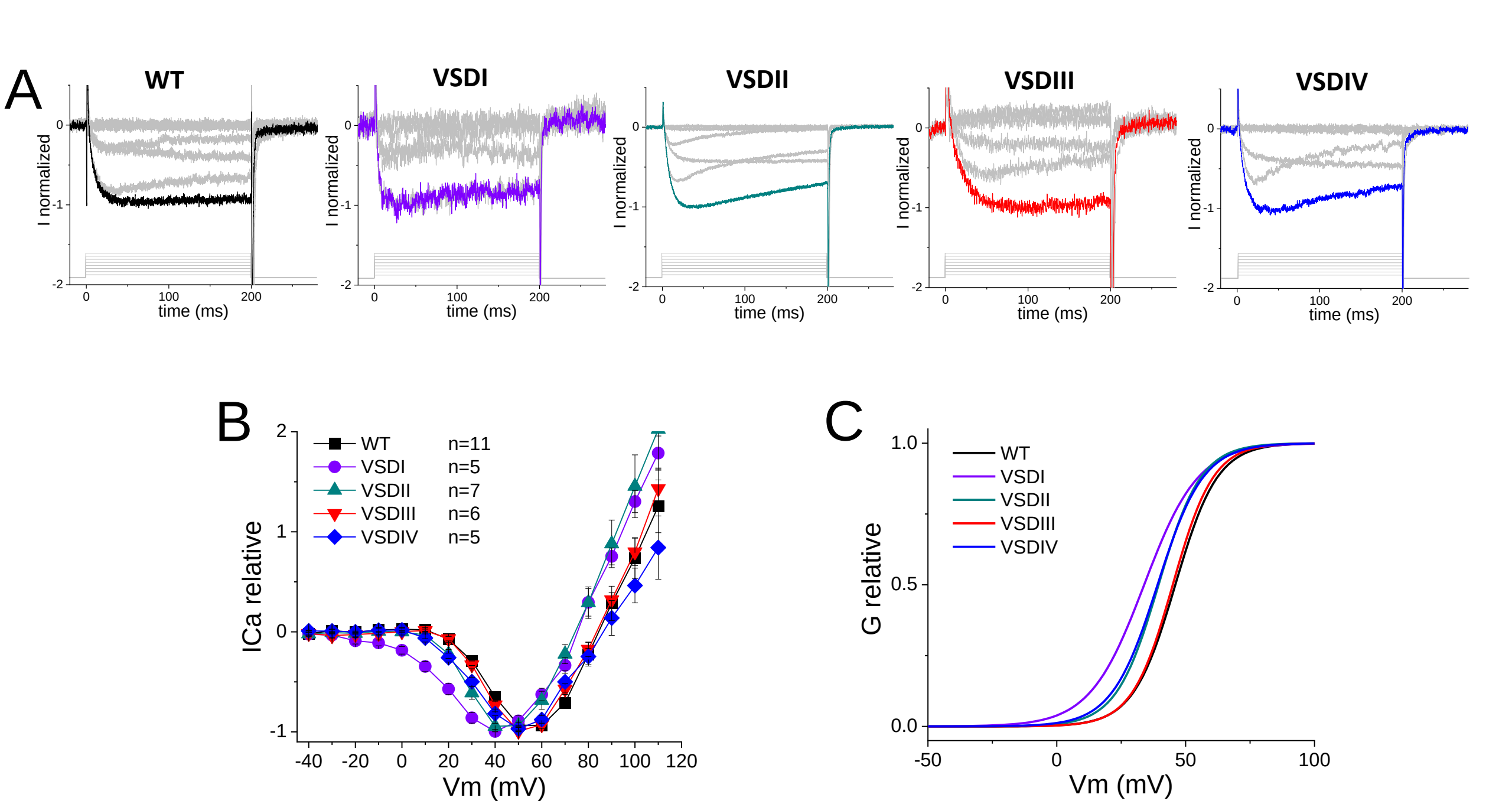
A
WT
VSDI
VSDII
VSDIII
VSDIV
I normalized
time (ms)
B
WT n=11
VSDI n=5
VSDII n=7
VSDIII n=6
VSDIV n=5
ICa relative
Vm (mV)
C
WT
VSDI
VSDII
VSDIII
VSDIV
G relative
Vm (mV)

Figure S4

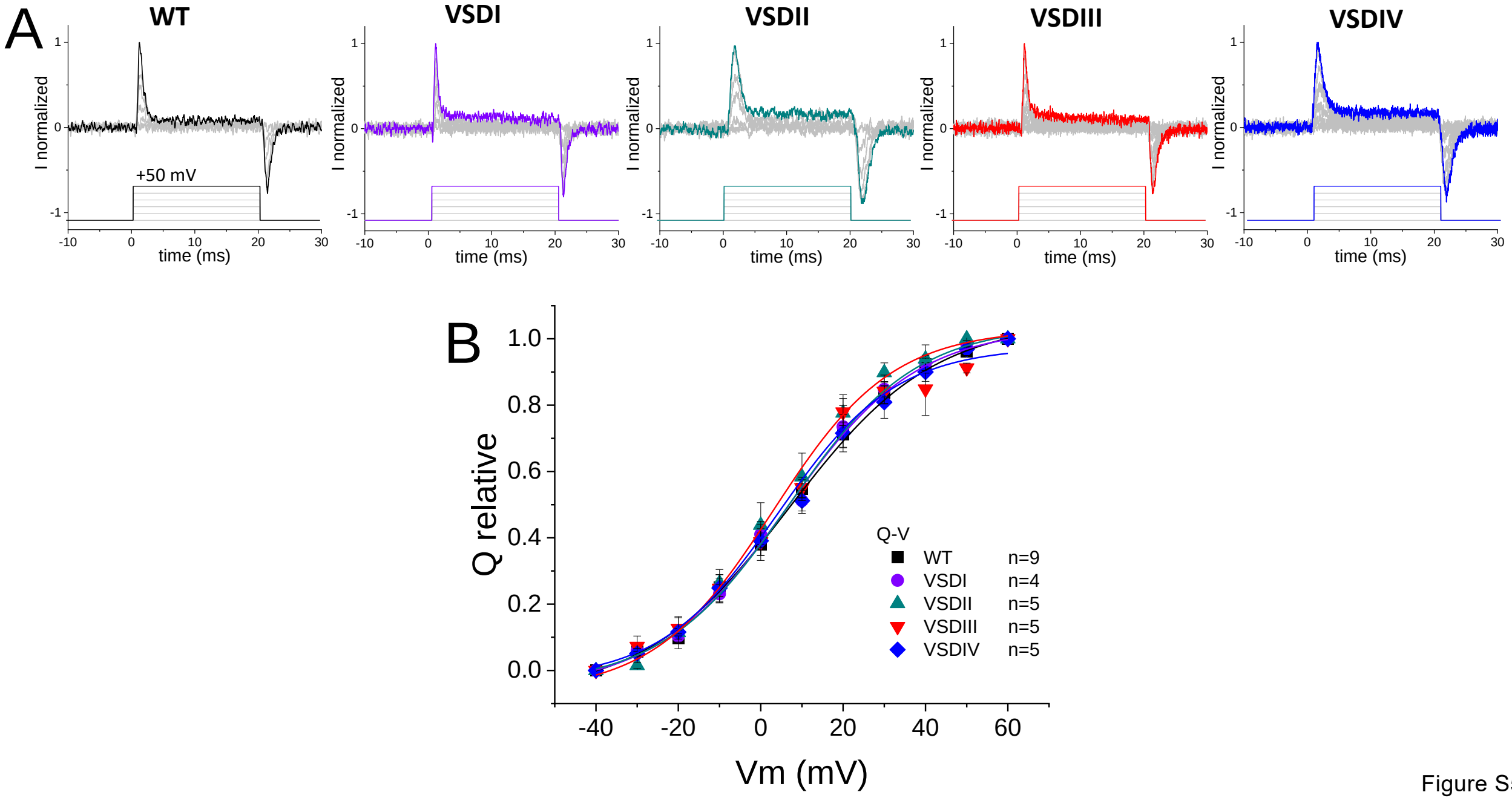
A
WT
VSDI
VSDII
VSDIII
VSDIV
I normalized
+50 mV
time (ms)
B
Q relative
Vm (mV)
Q-V
WT n=9
VSDI n=4
VSDII n=5
VSDIII n=5
VSDIV n=5

Figure S5

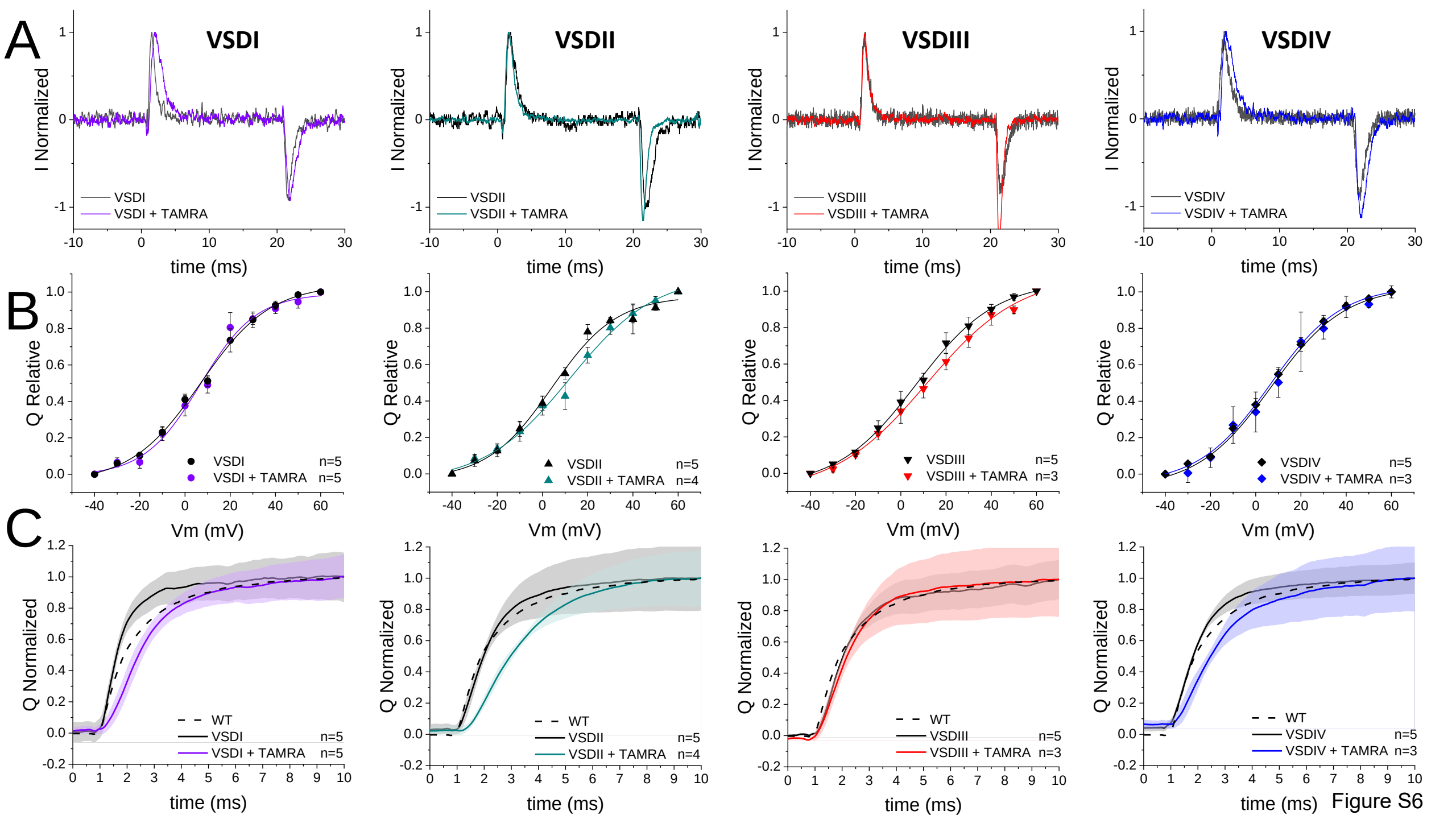
A
VSDI
VSDII
VSDIII
VSDIV
I Normalized
time (ms)
VSDI
VSDI + TAMRA
VSDII
VSDII + TAMRA
VSDIII
VSDIII + TAMRA
VSDIV
VSDIV + TAMRA
B
Q Relative
Vm (mV)
VSDI n=5
VSDI + TAMRA n=5
VSDII n=5
VSDII + TAMRA n=4
VSDIII n=5
VSDIII + TAMRA n=3
VSDIV n=5
VSDIV + TAMRA n=3
C
Q Normalized
time (ms)
WT
VSDI n=5
VSDI + TAMRA n=5
VSDII n=5
VSDII + TAMRA n=4
VSDIII n=5
VSDIII + TAMRA n=3
VSDIV n=5
VSDIV + TAMRA n=3

Figure S6

A

Single twitch response
before staining & stimulation

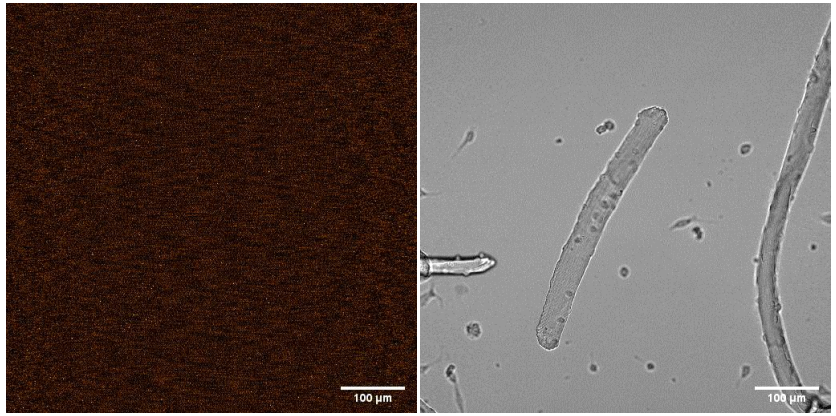

Before TAMRA trans

B

Single twitch response
after stimulation before washout

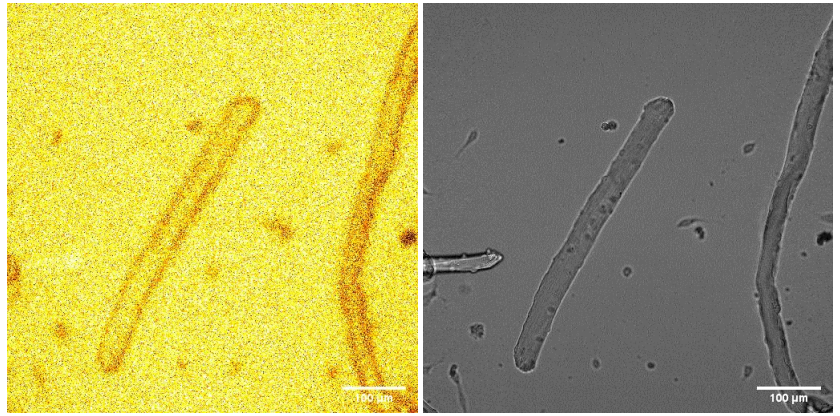

TAMRA trans

C

Single twitch response
10 min after washout & stimulation

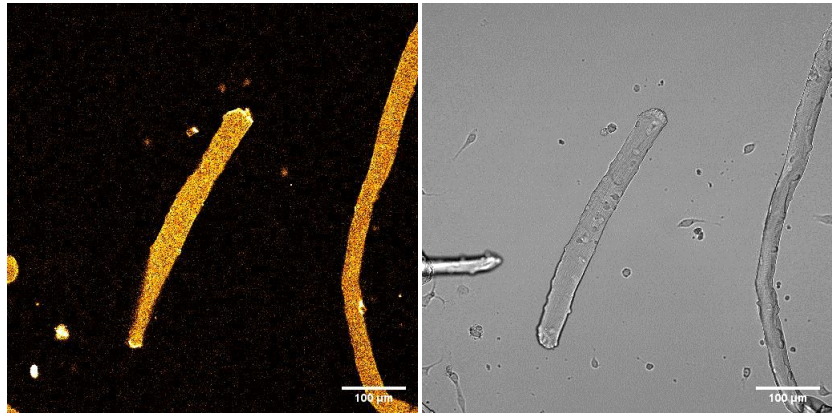

TAMRA trans

D

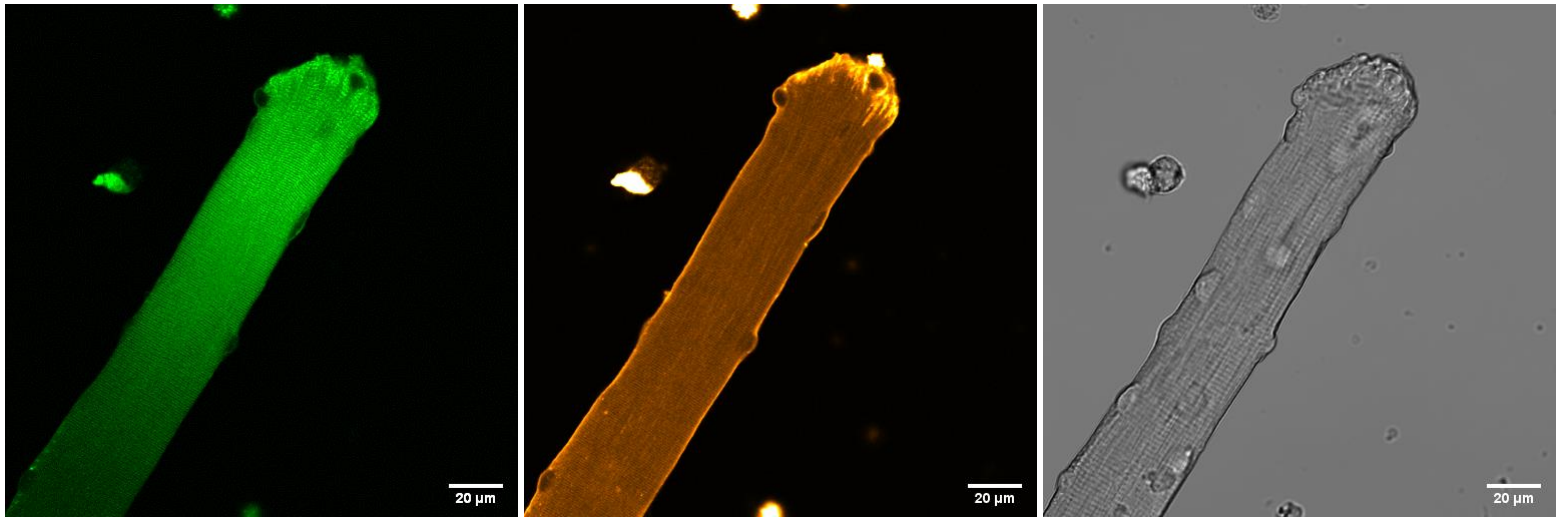

EGFP-$Ca_V1.1$ TAMRA trans

Figure S7

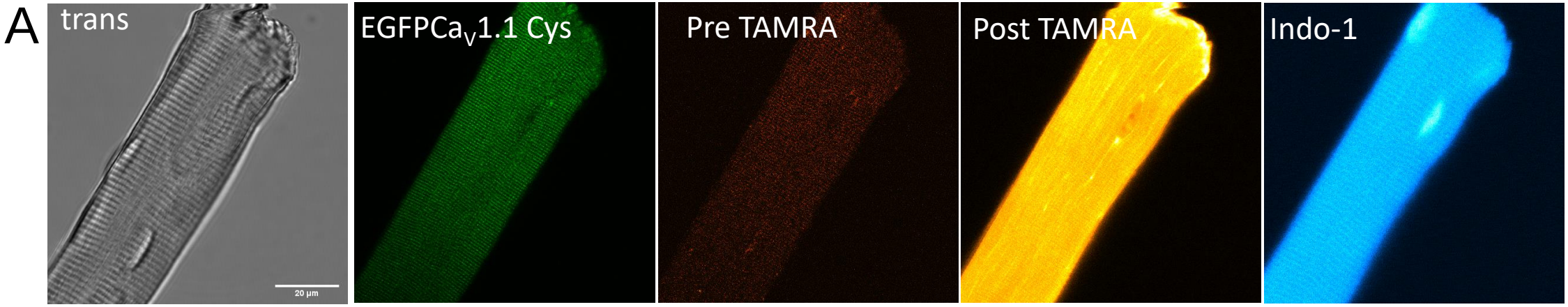
A
trans
20 µm
EGFPCaV1.1 Cys
Pre TAMRA
Post TAMRA
Indo-1
B
Pre TAMRA indo-1
Post TAMRA indo-1
time
C
pre TAMRA before stimulation
post TAMRA after stimulation
−ΔF/F0 indo-1420-460
time (ms)
peak −ΔF/F0
time to peak (ms)
pre TAMRA
post TAMRA
D
pre TAMRA before stimulation
post TAMRA after stimulation
First derivative of -ΔF/F0 (a.u.)
time (ms)
peak first derivative of -ΔF/F0 (a.u.)
pre TAMRA
post TAMRA

Figure S8

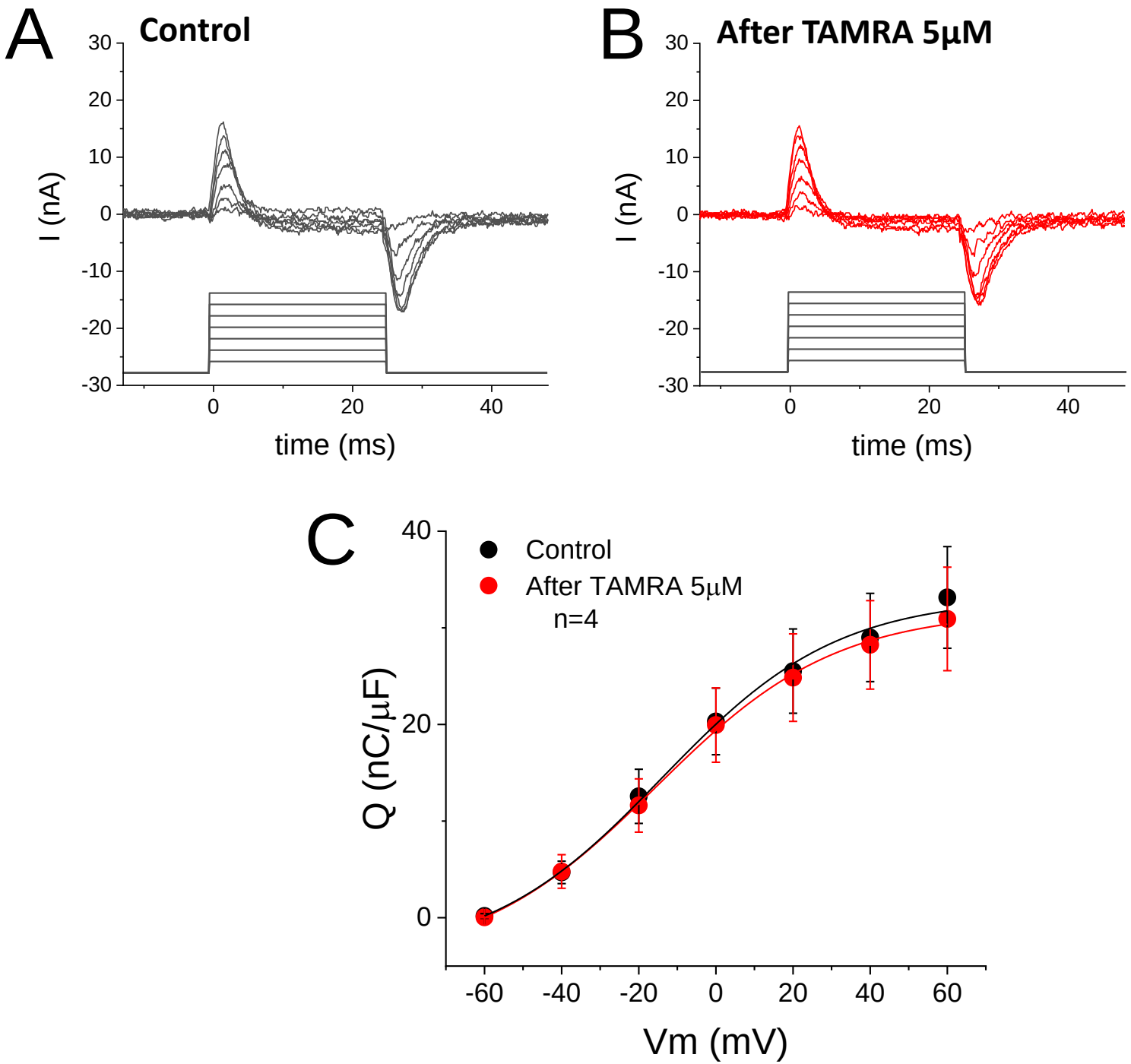
A
Control
I (nA)
time (ms)
B
After TAMRA 5µM
I (nA)
time (ms)
C
Control
After TAMRA 5µM
n=4
Q (nC/µF)
Vm (mV)

Figure S9

Table S1: Boltzmann's voltage dependence parameters of Ca2+ conductance for WT and VSDs Cys-engineered Cav1.1 channels.

	Ca^{2+} conductance		
Construct	V_{half} ***(mV)***	***K (mV)***	***n***
WT	46.9 ± 1.7	8.8 ± 0.6	11
VSDI	36.7 ± 1.6*	12.0 ± 0.7*	5
VSDII	39.8 ± 1.8	8.2 ± 0.4	7
VSDIII	46.8 ± 2.8	8.3 ± 0.8	6
VSDIV	39.3 ± 1.8	8.7 ± 0.4	5

Values are means ± SEM; *n*, number of cells evaluated. V_{half} defines the potential where G= 0.5 of G_{max} and *1/k* is a measure of the steepness of the *G-V* relationship. * indicates statistical difference for V_{half} and *k* (p=0.002 and p=0.006, respectively) from WT counterpart, tested using unpaired two-sample t-Test.

Table S2: Boltzmann's voltage dependence parameters of QON for WT and VSDs Cys-engineered Cav1.1 channels without or with TAMRA staining.

	Charge (Q_{ON})		
Construct	V_{half} ***(mV)***	***K (mV)***	***n***
WT	7.0 ± 2.5	16.1 ± 0.7	9
VSDI	13.3 ± 8.7	19.0 ± 5.6	4
VSDII	6.3 ± 3.8	16.6 ± 4.0	5
VSDIII	2.3 ± 2.7	15.2 ± 3.3	5
VSDIV	9.0 ± 3.8	18.6 ± 1.7	5
VSDI + TAMRA	7.3 ± 3.1	12.2 ± 3.3	5
VSDII + TAMRA	8.9 ± 3.9	14.9 ± 3.4	5
VSDIII + TAMRA	11.2 ± 6.0	21.0 ± 3.6	3
VSDIV + TAMRA	6.4 ± 7.4	13.0 ± 1.2	3

Values are means ± SEM; *n*, number of cells evaluated. V_{half} defines the potential where Q= 0.5 of Q_{max} and 1/*k* is a measure of the steepness of the *Q-V* relationship. No statistical differences were found between WT and Cys-engineered or between Cys-engineered and Cys-engineered + TAMRA (unpaired two-sample t-Test).

Table S3: Time dependence parameters of QON for WT and VSDs Cys-engineered Cav1.1 channels without or with TAMRA staining.

	Charge (Q_{ON}) kinetics		
Construct	t_{half} ***(ms)***	$\Delta t_{20\text{-}80}$ ***(ms)***	***n***
WT	1.76 ± 0.17	1.72 ± 0.43	9
VSDI	1.60 ± 0.07	2.19 ± 0.82	4
VSDII	1.86 ± 0.26	1.29 ± 0.38	5
VSDIII	1.93 ± 0.14	1.90 ± 0.38	5
VSDIV	1.80 ± 0.12	1.39 ± 0.15	5
VSDI + TAMRA	2.37 ± 0.28	2.03 ± 0.58	5
VSDII + TAMRA	2.83 ± 0.37	2.04 ± 0.34	5
VSDIII + TAMRA	2.12 ± 0.17	1.63 ± 0.32	3
VSDIV + TAMRA	2.32 ± 0.39	2.20 ± 0.51	3

Values are means ± SEM; *n*, number of cells evaluated. t_{half} defines the time where Q=0.5 and $\Delta t_{20\text{-}80}$ defines the time between Q=0.2 and Q=0.8; from the integration between Q_{20} ms to Q_{30} ms of the *Q-t* relationship. No statistical differences were found between WT and Cys-engineered channels or between Cys-engineered and Cys-engineered + TAMRA (unpaired two-sample t-Test).